Geothermometric study of Cr-spinels of peridotite mantle xenoliths from northern Victoria Land (Antarctica)

CRISTINA PERINELLI[1], FERDINANDO BOSI[2], GIOVANNI B. ANDREOZZI[2], AIDA M. CONTE[3]
PIETRO ARMIENTI[1]

[1]*Dipartimento di Scienze della Terra, Università di Pisa, via S. Maria 53, 56100 Pisa, Italy*

[2] *Dipartimento di Scienze della Terra, Sapienza Università di Roma, P.le Aldo Moro 5, 00185 Roma, Italy*

[3]*CNR-Istituto di Geoscienze e Georisorse, UOS Roma, P.le Aldo Moro 5, 00185 Roma, Italy*

Abstract

The crystal chemistry of Cr-spinels included in spinel peridotite mantle xenoliths from Baker Rocks and Greene Point (northern Victoria Land, Antarctica) has been studied by single-crystal structure refinement and electron microprobe analysis. All crystals are characterized by a dominance of Al ↔ Cr substitution with minor evidences of Mg ↔ Fe^{2+} substitution and pertain to the Mg-rich portion of the spinel *sensu stricto*-chromite join. The two groups of samples, Baker Rocks (BR) and Greene Point (GP), show distinct degree of cation order with the inversion parameter ranging from 0.17 to 0.20 for BR spinels and from 0.06 to 0.13 for GP crystals. Closure temperatures, computed by a geothermometer based on the $^{M}Al+^{T}Mg \leftrightarrow {}^{T}Al+^{M}Mg$ intracrystalline exchange, range from 883 to 911°C for BR spinels and from 592 to 675°C for GP spinels. We show that this difference is due to the higher concentration in Fe^{3+} in GP spinels that

enabled a faster kinetics of the intracrystalline cation ordering reaction, allowing the GP spinels to reach a higher degree of cation ordering and then lower closure temperatures.

Keywords: Cr-spinel, crystal structure, crystal chemistry, geothermometer, order-disorder kinetics, mantle xenoliths, Antarctica.

Introduction

Spinel-group minerals $(Mg,Fe^{2+})(Cr,Al,Fe^{3+})_2O_4$ are common accessory phases of basic and ultrabasic rocks both in the Earth's upper mantle and the crust. It is widely recognized that the structure and physical properties of spinels are governed by their formation conditions (temperature, pressure and chemical characteristics of the system), therefore spinels are widely exploited to reconstruct the physical parameters of their environment of origin (see, e.g., Irvine 1965, 1967; Dick and Bullen 1984; Barnes and Roeder 2001). The importance of this group of minerals has prompted extensive studies, many of which are aimed at defining intracrystalline order-disorder relationships and their dependence on equilibrium temperature, cooling history, and composition (e.g., Della Giusta et al. 1996; Princivalle et al. 1999; Andreozzi et al. 2000, 2001; Andreozzi and Princivalle 2002; Bosi et al. 2008; Lucchesi et al. 2010).

The general formula of spinel may be defined as AB_2O_4, where A and B are usually divalent and trivalent cations (respectively), although tetravalent cations can often occur (e.g., $FeTi_2O_4$). The spinel structure (space group $Fd\bar{3}m$) can be described as a slightly distorted cubic close-packed array of oxygen anions, in which the A and B cations are distributed in one-eighth of all tetrahedrally-coordinated sites (T) and half of all octahedrally-coordinated sites (M). With origin at $\bar{3}m$, T and M sites have fixed

coordinates (1/8 1/8 1/8 and 1/2 1/2 1/2 of the cell edge, respectively), and oxygen occupies a 3*m* point symmetry site with variable (*u u u*) coordinates. Modifications of T-O and M-O bond distances to accommodate various chemical compositions and/or cation ordering determine variations in the oxygen positional parameter *u* and the cell edge *a*. Two extreme site populations are possible: normal $^{T}(A)^{M}(B)_2O_4$ and inverse $^{T}(B)^{M}(AB)O_4$, both being ordered. However, natural spinels are commonly disordered and their cation distributions lie between these two extremes. The general formula defining the disordered cation distributions is $^{T}(A_{1-i}B_i)^{M}(A_iB_{2-i})O_4$ where the letter *i* represents the inversion parameter, that is the number of divalent cations at the M site. This parameter is strongly sensitive to temperature, and the inspection of literature reveals that for temperature increasing up to 1500 °C the value of *i* increases in normal spinels, from ca. zero to ca. 0.35, and decreases in inverse spinels, from ca. one to ca. 0.70 (Nell et al. 1989; O'Neill et al. 1992; Redfern et al. 1999; Andreozzi et al. 2000). In addition to temperature, the value of *i* is strongly dependent on spinel chemical composition and cation site preference. As for example, it is recognized that Cr^{3+} only occupies the spinel M site; Al and Cu^{2+} exhibit preference for the M site but are available to partly invert into the T site at high temperature; Fe^{3+} has no preference; Mg, Fe^{2+}, Mn^{2+} and Co^{2+} exhibit preference for the T site but are available to partly invert into the M site at high temperature; Zn only occupies the T site (Andreozzi et al. 2001; Andreozzi and Lucchesi 2002; Bosi et al. 2007; Hålenius et al. 2010; 2011; Fregola et al. 2012; D'Ippolito et al. 2012; Bosi et al. 2012). Consequently, at high temperature most of the cations are partially disordered between the T and M sites, but during the cooling path there is a progressive ordering of most of divalent cations at T and of Al at M. The temperature at which the rate of exchange slows to the point where the change is no longer detectable is defined as closure temperature (T_c). This implies that the

process of cation ordering relies on the rate at which spinel cooled, and is a track of thermal history of host rock. Slow cooling allows a strong cation ordering in spinel and determines low T_c, while fast cooling preserves the disordered state and determines high T_c (Princivalle et al. 1989; Della Giusta et al. 1996; Lucchesi and Della Giusta 1997; Lucchesi et al. 1998; Princivalle et al. 1999; Andreozzi et al. 2000; Andreozzi and Princivalle 2002; Lucchesi et al. 2010; Princivalle et al. 2012). In this regard, the presence of Cr in the spinel structure should not affect the T_c value, as shown by he invariance of T_c with respect to Cr in spinels coming from different localities (Uchida et al. 2005).

In this study, we report structural data of a set of Cr-spinels belonging to the peridotite mantle xenoliths from northern Victoria Land (Antarctica) carried to the surface by Cenozoic alkaline basic lavas. The structural parameters along with chemical data have been used to estimate the closure temperatures of the analyzed crystals in order to define the cooling history experienced by the northern Victoria Land spinel-peridotitic xenoliths.

Geological setting

The West Antarctic Rift System (WARS, Tessensohn and Wörner, 1991) is a region of lithospheric thinning revealed by a topographic trough running from the Antarctic Peninsula to the Ross Embayment-northern Victoria Land (NVL; Behrendt et al. 1991). The western flank of the rift in NVL is the back bone of the Transantarctic Mountains (TAM), representing the uplifted roots of the Early Paleozoic Ross Orogen. TAM uplift was practically amagmatic and it was accompanied by extensional tectonics in the adjacent Ross Sea Region during Late Cretaceous (e.g., Fitzgerald and Stump 1997 and reference therein).

Diffuse igneous activity has characterized the WARS since the Eocene. In northern Victoria Land, plutons, dyke swarms and volcanoes are emplaced in an area of about 400 × 80 km (Fitzgerald and Stump 1997; Rocchi et al. 2002; Tonarini et al. 1997). The volcanic products are grouped in the McMurdo Volcanic Group (Kyle 1990), while intrusive-subvolcanic varieties are collectively referred to as Meander Intrusive Group (Tonarini et al. 1997).

Spinel peridotite mantle xenoliths were brought to the surface by primitive alkaline magmas erupted from monogenetic cinder cones, at the margin of larger volcanoes or scattered on the crystalline basement, where the major active faults provided direct pathways to the surface (Salvini et al. 1997; Orlando et al. 1997). In particular, studies on xenoliths from two sites of NVL have revealed the heterogeneous nature of the underlying upper mantle, resulting from the combined effects of partial melting and metasomatic enrichment processes (Wörner 1999; Coltorti et al. 2004; Perinelli et al. 2006).

Experimental methods

Spinel crystals were separated by hand under a binocular microscope from a set of coarse-type peridotite xenoliths collected from monogenic cinder cones on the Ross Sea margin of WARS at Greene Point and Baker Rocks, two localities only 80 km apart. The xenoliths were selected on the basis of their refractory character, expressed in term of extent of melt extraction (i.e., degree of partial melting, F%, Table 1) and metasomatic signature. In Baker Rocks samples this latter is revealed by the occurrence of amphibole as dispersed grains or in vein (e.g., composite xenolith BR218, Table 1) and enrichments in major, minor (Fe and Ti, respectively) and incompatible trace elements. On the contrary, in Greene Point samples, the metasomatism is revealed by

the selective enrichment in incompatible elements of clinopyroxene (cryptic metasomatism; Table 1). Details on texture features and composition are reported in Perinelli et al. (2012 and references therein).

Single-crystal structural refinement

X-ray diffraction measurements were performed at Earth Sciences Department, Sapienza University of Rome, with a Bruker KAPPA APEX-II single-crystal diffractometer, equipped with CCD area detector (6.2 × 6.2 cm^2 active detection area, 512 × 512 pixels) and a graphite crystal monochromator, using MoKα radiation from a fine-focus sealed X-ray tube. The sample-to-detector distance was 4 cm. More than 4000 exposures per sample (step = 0.2°, time/step = 10 s) covering a full reciprocal sphere with a high redundancy of about 20 were collected. The orientation of the crystal lattice was determined from 500 to 1000 strong reflections ($I > 100\ \sigma_I$) evenly distributed in the reciprocal space, and used for subsequent integration of all recorded intensities. Final unit-cell parameters were refined by using Bruker's AXS SAINT program on reflections with $I > 10\ \sigma_I$ in the range $8° < 2\theta < 90°$. The intensity data were processed and corrected for Lorentz, polarization and background effects with APEX2 software program of Bruker AXS. The data were corrected for absorption using multi-scan method (SADABS). The absorption correction led to a significant improvement in R_{int}. No violation of $Fd\bar{3}m$ symmetry was noted. Sporadic appearance of forbidden space-group reflections was recognized as double reflections.

Structural refinements were done with the SHELXL program (Sheldrick 2008). Setting the origin at $\bar{3}m$, initial atomic positions for oxygen atoms were taken from the structure of spinel (Bosi et al. 2010). Variable parameters were overall scale factor, extinction coefficient, atomic coordinates, site scattering values expressed as mean

atomic number (m.a.n.), and atomic displacement factors. No chemical constraint was applied during the refinement. To obtain the best values of statistical indexes (*R*1 and *wR*2) the oxygen site was modeled with fully ionized oxygen scattering curves, while neutral curves were used for the cation sites. In detail, the T site was modeled considering the presence of Mg and Fe scattering factors, whereas the M site was modeled by Al and Cr scattering factors. Three full-matrix refinement cycles with isotropic displacement parameters for all atoms were followed by anisotropic cycles until convergence was attained, that is, when the shifts in all refined parameters were less than their estimated standard deviation. No correlation over 0.7 between parameters was observed at the end of refinement. Table 2 summarizes structural parameters and refinement details.

Chemical analysis

The chemical compositions of the crystals structurally refined were determined by means of electron microprobe (EMP) techniques, using a Cameca SX-50 instrument of the IGAG-CNR-Roma equipped with four wavelength dispersive spectrometers and a field emission electron gun operated at 15 kV accelerating potential and 15 nA beam current at a beam diameter of 1 μm. Cr-metal, Ni-metal, Al-corundum, Ti-rutile, Fe-magnetite, Mg-olivine, Mn-metal, Ca, Si-wollastonite were used as standards. The ZAF matrix correction procedure was applied for raw data reduction. Each element determination was accepted after checking that the intensity of analyzed standards before and after each measurement was within 1.00 ± 0.01. Precision for major elements (Mg, Fe, Al and Cr,) was usually within 1% of the actual amount present, and that of minor elements was within about 5%. A minimum of 6 spot analyses per crystal were performed (Table 3).

The contents of Fe^{2+} and Fe^{3+} in Table 3 were obtained from EMP chemical analyses by applying the Fe^{3+}/Fe_{tot} ratios determined by Mössbauer spectroscopy, as described in Perinelli et al. (2012).

Cation distribution

The intracrystalline cation distribution was obtained by an optimization program applying a minimization function in which both structural and chemical data (such as bond lengths and site-scattering in terms of equivalent electrons, i.e., mean atomic number) are taken into account. The minimization procedure has been presented and discussed previously (Carbonin et al. 1996; Andreozzi et al. 2001; Lavina et al. 2002; Bosi et al. 2004; Lenaz and Princivalle 2011; Della Giusta et al. 2011). For example, octahedral and tetrahedral bond lengths (M-O and T-O, respectively) can be calculated as the linear contribution of each cation multiplied by its ideal bond length, the latter refined on the basis of analysis of more than 250 spinel structural data from the literature (Lavina et al. 2002). For our samples, Cr, Ti^{4+} and Ni^{2+} were constrained to the M site, whereas Si and cation vacancies were constrained to T site. The optimized values of the variable cation fractions Al, Fe^{3+}, Mg and Fe^{2+} gave the final cation distributions (Table 4).

Results and discussion

Crystal chemistry

The investigated crystals are characterized by high contents of Al ranging from 1.03 to 1.76 atoms per formula unit (apfu), lower contents of Cr^{3+} ranging from 0.21 to 0.93 apfu, relatively high contents of Mg from 0.68 to 0.78 apfu, and lower contents of

both Fe^{2+} from 0.15 to 0.31 apfu, and Fe^{3+} from 0.04 to 0.09 apfu (Table 3). Four end-members are able to reproduce more than 90% of the observed chemical composition of the studied crystals (Table 4). Spinel *sensu stricto* ($MgAl_2O_4$) and chromite ($FeCr_2O_4$) are the most abundant components, while magnesiochromite ($MgCr_2O_4$) is significantly present only in samples GP6 and GP22; hercynite ($FeAl_2O_4$) characterizes samples GP42, BR218 and BR218*. As the spinel *sensu stricto* component is always dominant (ranging from 53 to 80%) and the (chromite+magnesiochromite) component is highly variable (7 to 41%), the studied crystals may be classified as Cr-rich spinel *sensu stricto* (Fig. 1). The intracrystalline cation distribution (Table 4) reveals that the inversion parameter *i* ranges from 0.06 to 0.20. In detail, the samples of Greene Point suite show lower inversion degree (0.06-0.13) than the samples of Baker Rocks suite (0.17-0.20). The number of cation vacancies is very low and can be considered as negligible in BR samples (< 0.01 per formula unit, pfu), but it is relevant in GP samples (up to 0.03 pfu). The occurrence of cation vacancies may be explained by the post-formation process of progressive oxidation of Fe^{2+} to Fe^{3+} described by the mechanism: $2Fe^{2+} + ½O_2 \rightarrow 2Fe^{3+} + O^{2-}$ + vacancy (O'Reilly and Banerjee 1967; Menegazzo et al. 1997; Bosi et al. 2004; Quintiliani et al. 2006). In the studied samples such a mechanism is supported by the concomitant increase of cation vacancies and Fe^{3+} contents, in a ratio close to 1:2 (Fig. 2).

The unit-cell parameter increases with increasing Cr (Fig. 3). The bond distances T-O and M-O change as a function of Al at the T and M sites, according to the relations:

$$\text{T-O} = 1.966 - 0.165 \times {}^{T}\text{Al} \qquad (r^2 = 0.97)$$

$$\text{M-O} = 1.993 - 0.037 \times {}^{M}\text{Al} \qquad (r^2 = 0.92)$$

The oxygen positional parameter *u* marks a significant difference between GP and BR spinels: the *u* value observed for BR spinels ranges from 0.2623 to 0.2626, whereas, for

GP spinels, *u* varies from 0.2628 to 0.2633 (Table 2).

Intracrystalline geothermometry

The geothermometer described by Princivalle et al. (1999) allows to obtain the closure temperature for spinel from its cation distribution. It is based on the temperature-dependent intracrystalline exchange reaction $^{M}Al + {}^{T}Mg \leftrightarrow {}^{T}Al + {}^{M}Mg$. The closure temperature T_c is obtained by the relation:

$$T_c = 6640\ [{}^{T}Al/Al_{tot} + 0.101(1 - {}^{T}Mg - {}^{T}Al) + 0.041(2 - {}^{M}Al - {}^{M}Mg)]$$

where the coefficients take into account the compositional influence of the other cations. The uncertainty associated with this geothermometer is ±20 °C. The calculated T_c are listed in Table 5. The calculated T_c values obtained for spinels hosted in BR peridotite xenoliths range from 883 to 911 °C, whereas T_c values obtained for GP spinels range from 592 to 675 °C, remarkably lower than previous ones.

As stressed by Lucchesi et al. (2010), it should be noted that each of these values represents the temperature at which the intracrystalline exchange reaction practically stopped. The closure temperature is linked to the kinetics of cooling events, which among other factors depend on cooling rate of the lava hosting the xenoliths, on the sizes of the xenoliths and on the position of the crystal within the xenoliths. In fact, it is expected that large xenoliths will cool more slowly than small ones and crystals close to xenolith rims will close at a higher temperature than those located in the inner parts. Thus, crystals initially at the same equilibrium temperature within the mantle may follow different cooling paths and therefore show different closure temperatures. In this view, only the T_c's recorded by the BR spinels (~900 °C) are in agreement with equilibrium temperatures (907-933 °C; Table 5) calculated by the intercrystalline

olivine-spinel geothermometer of Ballhaus et al. (1991) and both are close to the range of equilibrium temperatures estimated for NVL lithospheric mantle (~900-1100 °C; Armienti and Perinelli 2010). This indicates that the cooling rate of these xenoliths was so fast as to prevent the triggering of the intracrystalline Mg-Al ordering reaction in the spinel. On the contrary, the low T_c's recorded by GP spinels (592-675 °C; Table 5), and their discrepancy with olivine-spinel intercrystalline temperatures (985-1113°C; Table 5), would suggest that GP xenoliths underwent cooling rates slower than BR xenoliths, even though their similarities in host rocks and xenolith sizes point to comparable fast cooling histories.

Applicability of spinel intracrystalline geothermometry to mantle xenoliths

The differences in calculated closure temperatures between BR and GP spinels reflect the observed differences in the values of *i* parameter (0.17-0.20 and 0.06-0.13 for BR and GP samples, respectively) and namely the differences of the crystal-chemical relationships between *u* parameter and Cr content (Fig. 4). In this regard, Lenaz et al. (2010) investigated on the equilibration processes involved in the cooling history of the lherzolite mantle peridotites of Ronda (Spain). They observed that for similar Cr content, *u* values of Cr-spinels from peridotite mantle xenoliths are always lower than those of Cr-spinels from mantle peridotite massifs. Moreover, they demonstrated that in the peridotite massifs the variation in Cr content of spinels is linearly related to the change in the *u* parameter, on the contrary in spinels from xenoliths no correlation was found between Cr and *u*. Lenaz et al. (2010) related the observed different behaviors to the cooling path experienced by the mantle rocks (massif/xenolith): slow cooling for a peridotite massif during its sluggish (million years) ascent into the Earth crust or fast cooling for xenoliths (minutes/hours) linked to the host lava chilling after its

emplacement at the surface. They also reported that the intracrystalline closure temperatures calculated from Cr-spinels of mantle xenoliths are usually higher (T_c = 700-1000°C) than those derived from spinels of mantle peridotite bodies/massifs (T_c < 700°C).

In our case, as expected for spinels from mantle xenoliths, BR samples show T_c ~ 900°C and do not display relationships between Cr content and the *u* parameter. On the contrary, GP spinels exhibit lower T_c values (< 700°C) and a linear correlation between the Cr content and *u* parameter, whose trend approaches that commonly shown by spinels from peridotite bodies/massifs (Fig. 4). Both the T_c values and the *u*-Cr relationships determined for these spinels are in contrast with the rapid cooling of lava that carried the GP xenoliths from the mantle. Therefore, differences in T_c and *u*-Cr relationships between GP and BR spinels must be attributed to the respective diversities in crystal chemistry.

Experimental studies on spinels have demonstrated that the kinetics of intracrystalline cation order-disorder is influenced by Fe^{3+} and Cr contents as well as by non-stoichiometry (O'Neill 1994 1997; Harrison and Putnis 1999; Princivalle et al. 2006; Martignago et al. 2006; Princivalle et al. 2012). In particular, the presence of Fe^{3+} fosters the intracrystalline cation ordering process, because it was established that, in Fe^{3+}-rich aluminate spinels, the Mg-Fe^{3+} site exchange proceeds at higher speed and to lower temperature than the Mg-Al exchange (Martignago et al. 2006). The main compositional difference between GP and BR spinels is in Fe^{3+} content. Even for the same Cr#, the GP spinels are significantly enriched in Fe^{3+} compared to BR samples due to oxidation and creation of cation vacancies (Table 3). Consequently, since both GP and BR suites experienced the similar cooling histories, we argue that the higher concentration in Fe^{3+} and non-stoichiometry of GP spinels permitted cation ordering to

lower temperature, and thus recording lower T_c, during the host lava cooling.

The present study confirms that intracrystalline Mg-Al distribution between the T and M sites in the spinel structure is a very sensitive recorder of temperature variation. In the present case, when this approach was applied to non-stoichiometric Cr-spinels from mantle xenoliths, in spite of the rapid cooling of magma that carried the xenoliths, the closure temperatures obtained did not record the thermal conditions within the mantle, but reflect phases of the cooling of the xenolith-host lava. This implies that a full chemical and structural characterization along with accurate crystal-chemical analysis is needed in order to solve problems concerning the cooling rate of spinel-hosting rocks.

Acknowledgments

We gratefully acknowledge funds provided by the project PRIN 2010-11 ‘‘GEO-TECH’’ and Università Sapienza 2012 “Studio cristallochimico di spinelli appartenenti alle serie $(Mg,Fe)_2TiO_4$, $(Mg,Cu)Al_2O$ e $(Mg,Fe)(Al,Cr)_2O_4$ finalizzato ad applicazioni geologiche e tecnologiche”. We thank the Technical Editor, the Associate Editor C. Lesher, S. Barnes and one anonymous reviewer for their careful work and their very constructive comments. M. Serracino (CNR-IGAG) kindly helped during EMP analyses.

References Cited

Andreozzi, G.B., Princivalle, F., Skogby, H. and Della Giusta, A. (2000) Cation ordering and structural variations with temperature in $MgAl_2O_4$ spinel: an X- ray single crystal study. American Mineralogist, 85, 1164–1171. Erratum, 86, 204.

Andreozzi, G.B., Lucchesi, S., Skogby, H. and Della Giusta, A. (2001) Composition dependence of cation distribution in some synthetic $(Mg,Zn)(Al,Fe^{3+})_2O_4$ spinels. European Journal of Mineralogy, 13, 391-402.

Andreozzi G.B. and Lucchesi S. (2002) Intersite distribution of Fe^{2+} and Mg in the spinel (sensu stricto)-hercynite series by single-crystal X-ray diffraction. American Mineralogist, 87, 1113-1120.

Andreozzi, G.B. and Princivalle, F. (2002) Kinetics of cation ordering in synthetic $MgAl_2O_4$ spinel. American Mineralogist, 87, 838–844.

Armienti, P. and Perinelli C. (2010) Cenozoic thermal evolution of lithospheric mantle in northern Victoria Land (Antarctica): Evidences from mantle xenoliths. Tectonophysics, 486, 28–35.

Ballhaus, C., Berry, R.F. and Green, D.H. (1991) High pressure experimental calibration of the olivine-orthopyroxene-spinel oxygen barometer: implications for the oxidation state of the upper mantle. Contributions to Mineralogy and Petrology, 107, 27–40, corrected in Contributions to Mineralogy and Petrology (1991), 108, 384–384 and Contributions to Mineralogy and Petrology (1994), 118, 109.

Barnes, S.J. and Roeder, P.L., (2001) The range of Spinel Compositions in Terrestrial Mafic and Ultramafic Rocks, Journal of Petrology, Volume 42, pages 2279-2302.

Basso, R., Comin-Chiaramonti, P., Della Giusta, A. and Flora, O. (1984) Crystal chemistry of four Mg-Fe-Al-Cr spinels from the Balmuccia peridotite (Western Italian Alps). Neues Jahrbuch für Mineralogie Abhlandungen, 150, 1-10.

Behrendt, J.C., LeMausurier, W., Cooper, A.K., Tessensohn, F., Tréhu, A. and Damaske, D. (1991) Geophysical studies of the West Antarctic Rift System. Tectonics, 10(6), 1257-1273

Bosi, F., Andreozzi G.B., Ferrini, V. and Lucchesi, S. (2004) Behavior of cation vacancy in kenotetrahedral Cr-spinels from Albanian eastern belt ophiolites. American Mineralogist, 89, 1367-1373

Bosi, F., Hålenius, U., Andreozzi, G.B., Skogby, H. and Lucchesi, S. (2007) Structural refinement and crystal chemistry of Mn-doped spinel: A case for tetrahedrally coordinated Mn^{3+} in an oxygen-based structure. American Mineralogist, 92, 27-33.

Bosi, F., Hålenius, U. and Skogby, H. (2008) Stoichiometry of synthetic ulvöspinel single crystals. American Mineralogist, 93, 1312–1316.

Bosi, F., Hålenius, U. and Skogby, H. (2010) Crystal chemistry of the $MgAl_2O_4$-$MgMn_2O_4$-$MnMn_2O_4$ system: Analysis of structural distortion in spinel and hausmannite-type structures. American Mineralogist, 95, 602-607.

Bosi, F., Hålenius, U., D'Ippolito, V. and Andreozzi, G.B. (2012) Blue spinel crystals in the $MgAl_2O_4$-$CoAl_2O_4$ series: II. Cation ordering over short-range and long-range scales. American Mineralogist, 97, 1834-1840.

Carbonin, S., Russo, U. and Della Giusta, A. (1996) Cation distribution in some natural spinels from X-ray diffraction and Mössbauer spectroscopy. Mineralogical Magazine, 60, 355-368.

Carraro, A. (2003) Crystal chemistry of Cr-spinels from a suite of spinel peridotite mantle xenoliths from the Predazzo Area (Dolomites, Northern Italy). European Journal of Mineralogy, 15, 681-688.

Coltorti, M., Beccaluva, L., Bonadiman, C., Faccini, B., Ntaflos, T. and Siena F. (2004) Amphibole genesis via metasomatic reaction with clinopyroxene in mantle xenoliths from Victoria Land, Antarctica. Lithos, 75, 115-139.

Della Giusta, A., Princivalle, F., and Carbonin, S. (1986) Crystal chemistry of a suite of

natural Cr-bearing spinels with 0.15 < Cr < 1.07. Neues Jahrbuch für Mineralogie Abhlandungen, 155, 319–330.

Della Giusta, A., Carbonin, S. and Ottonello, G. (1996) Temperature-dependent disorder in a natural Mg-Al-Fe^{2+}-Fe^{3+}-spinel. Mineralogical Magazine, 60, 603–616

Della Giusta, A., Carbonin, S., and Russo, U. (2011) First occurrence of titanomagnetites from the websterite dykes within Balmuccia peridotite (Ivrea-Verbano zone): crystal chemistry and structural refinement. Periodico di Mineralogia, 80, 1-17.

Dick, H.J.B. and Bullen, T. (1984) Chromian spinel as petrogenetic indicator in abyssal and alpine type peridotites and spatially associated lavas. Contributions to Mineralogy and Petrology, 86, 54-76

Fitzgerald, P.G. and Stump, E. (1997) Cretaceous and Cenozoic episodic denudation of the Transantarctic Mountains, Antarctica: new constraints from apatite fission track thermochronology in the Scott Glacier region. Journal of Geophysical Research, 102 (B4), 7747-7765.

Fregola, R.A., Bosi, F., Skogby, S. and Hålenius, U. (2012) Cation ordering over short-range and long-range scales in the $MgAl_2O_4$-$CuAl_2O_4$ series. American Mineralogist, 97, 1821-1827.

Harrison, R.J. and Putnis, A. (1999) Determination of the mechanism of cation ordering in magnesioferrite (MgFe2O4) from the time- and temperature-dependence of magnetic susceptibility. Physics and Chemistry of Minerals, 26, 322–332.

Hålenius U., Andreozzi G.B. and Skogby H. (2010). Structural relaxation around Cr^{3+} and the red-green color change in the spinel (sensu stricto)–magnesiochromite

($MgAl_2O_4$–$MgCr_2O_4$) and gahnite–zincochromite ($ZnAl_2O_4$–$ZnCr_2O_4$) solid solution series. American Mineralogist, 95, 456-462.

Hålenius, U., Bosi, F. and Skogby, H. (2011) A first record of strong structural relaxation of TO_4 tetrahedra in a spinel solid solution. American Mineralogist, 96, 617-622.

Hellebrand, E., Snow, J.E., Dick, H.J.B. and Hofmann, A.W. (2001) Coupled major and trace elements as indicators of the extent of melting in mid-ocean-ridge peridotites. Nature, 410, 677–681.

Irvine, T.N. (1965) Chromian spinel as a petrogenetic indicator, Canadian Journal of Earth Sciences, Volume 2, pages 648-672.

Irvine, T.N. (1967) Chromian spinel as a petrogenetic indicator, Canadian Journal of Earth Sciences, Volume 4, pages 71-103.

Kyle, P.R. (1990) McMurdo Volcanic Group-Western Ross Embayment: Introduction. In: LeMasurier, W.E and Thomson, J.W. (eds) Volcanoes of the Antarctic Plate and Southern Oceans American Geophysical Union Washington DC, pp 19-25

Lavina, B., Salviulo, G. and Della Giusta, A. (2002) Cation distribution and structure modeling of spinel solid solutions. Physics and Chemistry of Minerals, 29, 10–18.

Lenaz, D. and Princivalle, F. (2011) First occurrence of titanomagnetites from the websterite dykes within Balmuccia peridotite (Ivrea-Verbano zone): crystal chemistry and structural refinement. Periodico di Mineralogia, 80, 19-26.

Lenaz, D., De Min, A., Garuti, G., Zaccarini, F. and Princivalle, F. (2010) Crystal chemistry of Cr-spinels from the lherzolite mantle peridotite of Ronda (Spain). American Mineralogist, 95, 1323–1328.

Lucchesi, S., Bosi, F. and Pozzuoli, A. (2010) Geothermometric study of Mg-rich spinels from the Somma-Vesuvius volcanic complex (Naples, Italy). American

Mineralogist, 95, 617-621.

Martignago, F., Andreozzi, G.B. and Dal Negro, A. (2006) Thermodynamics and kinetics of cation ordering in some natural and synthetic $Mg(Al,Fe^{3+})_2O_4$ spinels from in situ HT X-ray diffraction. American Mineralogist, 91, 306-312.

Menegazzo, G., Carbonin, S. and Della Giusta, A. (1997) Cation and vacancy distribution in an artificially oxidized natural spinel. Mineralogical Magazine, 61, 411-421.

Nédli, Zs., Princivalle, F., Lenaz, D. and T-th, T.M. (2008) Crystal chemistry of clinopyroxene and spinel from mantle xenoliths hosted in Late Mesozoic lamprophyres (Villány Mts., South Hungary). Neues Jahrbuch für Mineralogie Abhandlungen, 185, 1-10.

Nell, J., Wood, B.J., and Mason, T.O. (1989) High temperature cation distributions in Fe_3O_4-$MgAl_2O_4$-$MgFe_2O_4$-$FeAl_2O_4$ spinels from thermopower measurements. American Mineralogist, 74 , 339-35l.

O'Neill, H.St.C. (1994) Kinetics of cation order-disorder in MgFe2O4 spinel. European Science Foundation Program on Kinetic Processes in Minerals and Ceramics, Proc. Workshop on Kinetics of Cation Ordering, Cambridge, England.

O'Neill, H.St.C. (1997) Kinetics of the intersite cation exchange in MgAl2O4 spinel: the influence of nonstoichiometry. Seventh Annual V.M. Goldschmidt Conference, Tucson, Arizona, June 2–6.

O'Neill H.St.C., Annersten, H. and Virgo D. (1992) The temperature dependence of the cation distribution in magnesioferrite ($MgFe_2O_4$) from powder XRD structural refinements and Mössbauer spectroscopy. American Mineralogist, 77,725-740.

Orlando, A., Armienti, P., Conticelli, S., Vagelli, G. and Manetti, P. (1997) Petrologic investigations on the primitive Cainozoic lavas of Northern Victoria Land,

Antarctica. In: Ricci C.A. (ed) The Antarctic Region: Geological evolution and processes, Terra Antarctica Publication, Siena, Italy, pp 523-530-

Perinelli, C., Armienti, P. and Dallai, L. (2006) Geochemical and O-isotope constraints on the evolution of lithospheric mantle in the Ross Sea rift area (Antarctica). Contributions to Mineralogy and Petrology, 151, 245-266.

Perinelli, C., Andreozzi, G.B., Conte, A.M., Oberti, R. and Armienti P. (2012) Redox state of subcontinental lithospheric mantle and relationships with metasomatism: insights from spinel-peridotites from northern Victoria Land (Antarctica). Contributions to Mineralogy and Petrology, 164, 1053-1067.

Princivalle, F., DellaGiusta, A. and Carbonin, S. (1989) Comparative crystal chemistry of spinels from some suites of ultramafic rocks. Mineralogy and Petrolology, 40, 117-126.

Princivalle, F., Della Giusta, A., De Min, A. and Piccirillo, E.M. (1999) Crystal chemistry and significance of cation ordering in Mg-Al rich spinels from high grade hornfels (Predazzo-Monzoni, NE Italy). Mineralogical Magazine, 63, 257–262.

Princivalle, F., Martignago, F. and Dal Negro, A. (2006) Kinetics of cation ordering in natural $Mg(Al,Cr^{3+})_2O_4$ spinels. American Mineralogist, 91, 313–318.

Princivalle, F., Martignago F., Nestola, F. and Dal Negro A. (2012) Kinetics of cation ordering in synthetic $Mg(Al, Fe^{3+})_2O_4$ spinels. European Journal of Mineralogy, 24, 633-643.

Quintiliani, M., Andreozzi, G.B. and Graziani, G. (2006) Fe^{2+} and Fe^{3+} quantification by different approaches and f_{O2} estimation for Albanian Cr-spinels. American Mineralogist, 91, 907-916.

Redfern, S.A.T., Harrison, R.J., O'Neill, H.st:C. and Wood, D.R.R. (1999): Thermodynamics and kinetics of cation ordering in MgAl2O4 spinel up to 1600°C from in situ neutron diffraction. American Mineralogist, 84, 299-310.

Rocchi, S., Armienti, P., D'Orazio, M., Tonarini, S., Wijbrans, J. and Di Vincenzo, G.D. (2002) Cenozoic magmatism in the western Ross Embayment: role of mantle plume vs. plate dynamics in the development of the West Antarctic Rift System. Journal of Geophysical Research, 107 B7, doi:10.1029/(2001).

Salvini, F., Brancolini, G., Busetti, M., Storti, F., Mazzarini, F. and Coren, F. (1997) Cenozoic geodynamics of the Ross Sea region of Antarctica: Crustal extension, intraplate strike-slip faulting and tectonic inheritance. Journal of Geophysical Research, 102, 24669-24696.

Sheldrick, G.M. (2008) A short history of SHELX. Acta Crystallographica, A64, 112-122.

Tessensohn, F. and Wörner, G. (1991) The Ross Sea Rift System (Antarctica): Structure, evolution and analogues. In: Thomson MRA, Crame. J.A. and Thomson. J.W. (Ed.) "Geological evolution of Antarctica" Cambridge University Press: pp 273-277.

Tonarini, S., Rocchi, S., Armienti, P. and Innocenti, F. (1997) Constraints on timing of Ross Sea rifting inferred from Cainozoic intrusions from Northern Victoria Land, Antarctica. VII ISAES The Antarctic Region: Geological evolution and processes: pp 511-522.

Uchida, H., Lavina, B., Downs, R.T. and Chesley, J. (2005) Single-crystal X-ray diffraction of spinels from the San Carlos Volcanic Field, Arizona: Spinel as a geothermometer. American Mineralogist, 90, 1900-1980.

Wörner, G. (1999) Lithospheric dynamics and mantle sources of alkaline magmatism of the Cenozoic West Antarctic Rift System. Global Planet Change 23:61-77.

Figure captions

Figure 1. Spinel classification diagram. GP = Greene Point, BR = Baker Rocks, BR218* = portion of the lherzolite adjacent to amphibole-bearing vein.

Figure 2. Ferric iron (Fe^{3+}) vs. vacancy amount for Greene Point and Baker Rocks spinels. Symbol dimensions are proportional to ±2σ. GP = Greene Point, BR = Baker Rocks, BR218* = portion of the lherzolite adjacent to amphibole-bearing vein.

Figure 3. Unit-cell parameter *a* (Å) vs. Cr content (apfu). Symbol dimensions are proportional to ±2σ. GP = Greene Point, BR = Baker Rocks, BR218* = portion of the lherzolite adjacent to amphibole-bearing vein.

Figure 4. Oxygen positional parameter *u vs.* Cr content (apfu).

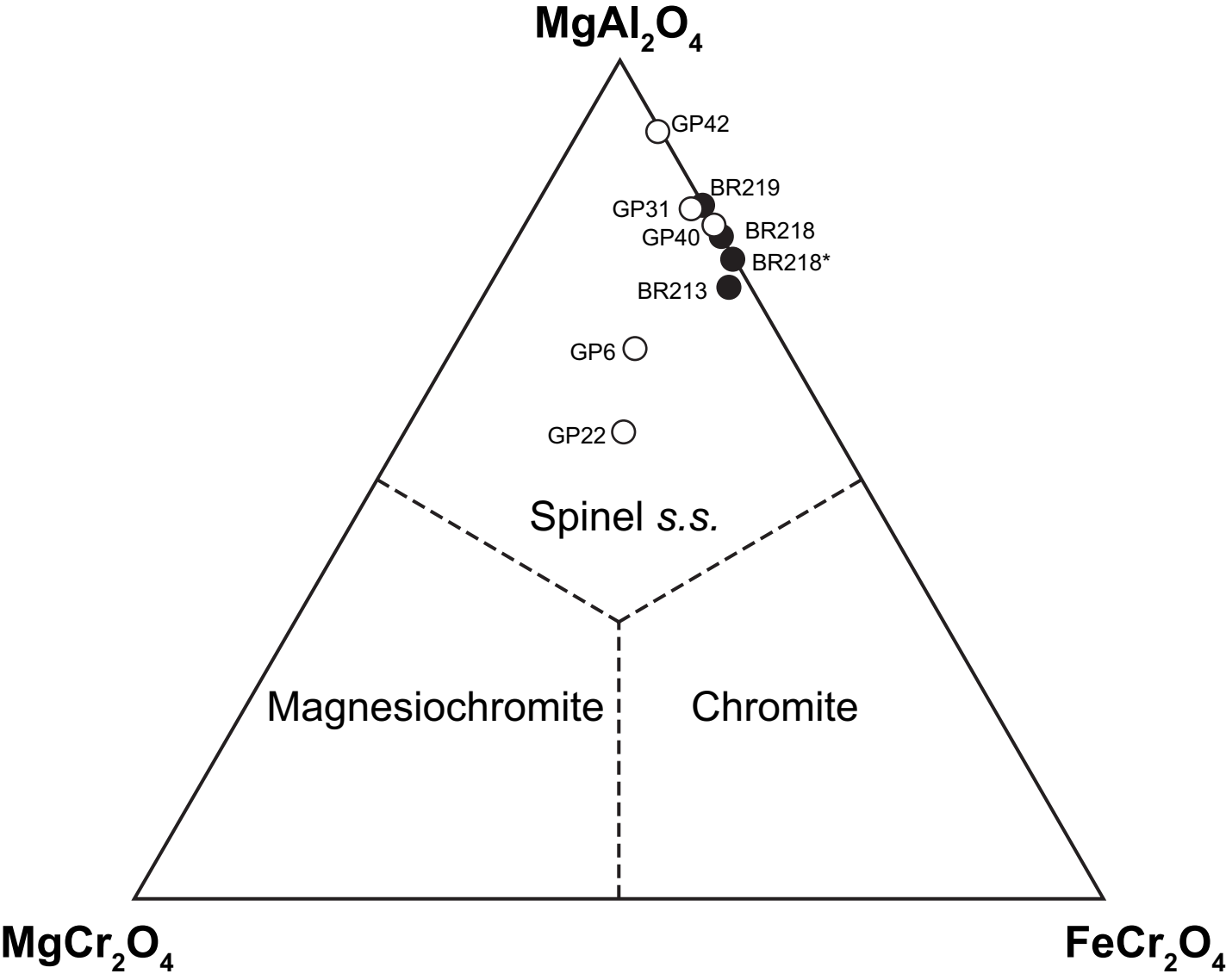
MgAl2O4
GP42
BR219
GP31
GP40
BR218
BR218*
BR213
GP6
GP22
Spinel s.s.
Magnesiochromite
Chromite
MgCr2O4
FeCr2O4

Figure 1

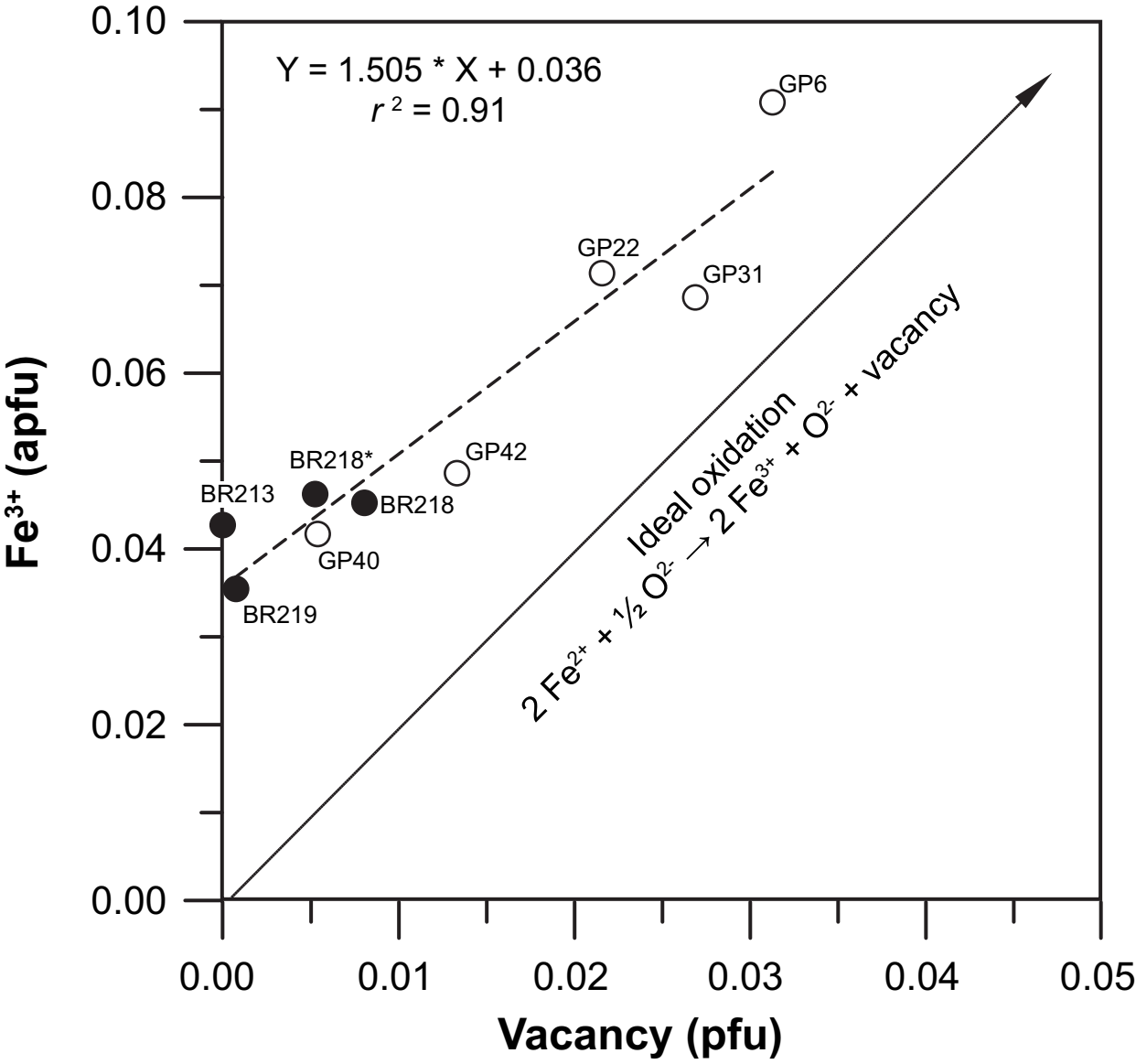
Y = 1.505 * X + 0.036
r 2 = 0.91
GP6
GP22
GP31
GP42
BR218*
BR213
BR218
GP40
BR219
Ideal oxidation
2 Fe2+ + ½ O2- → 2 Fe3+ + O2- + vacancy
Fe3+ (apfu)
Vacancy (pfu)
0.00
0.02
0.04
0.06
0.08
0.10
0.00
0.01
0.02
0.03
0.04
0.05

Figure 2

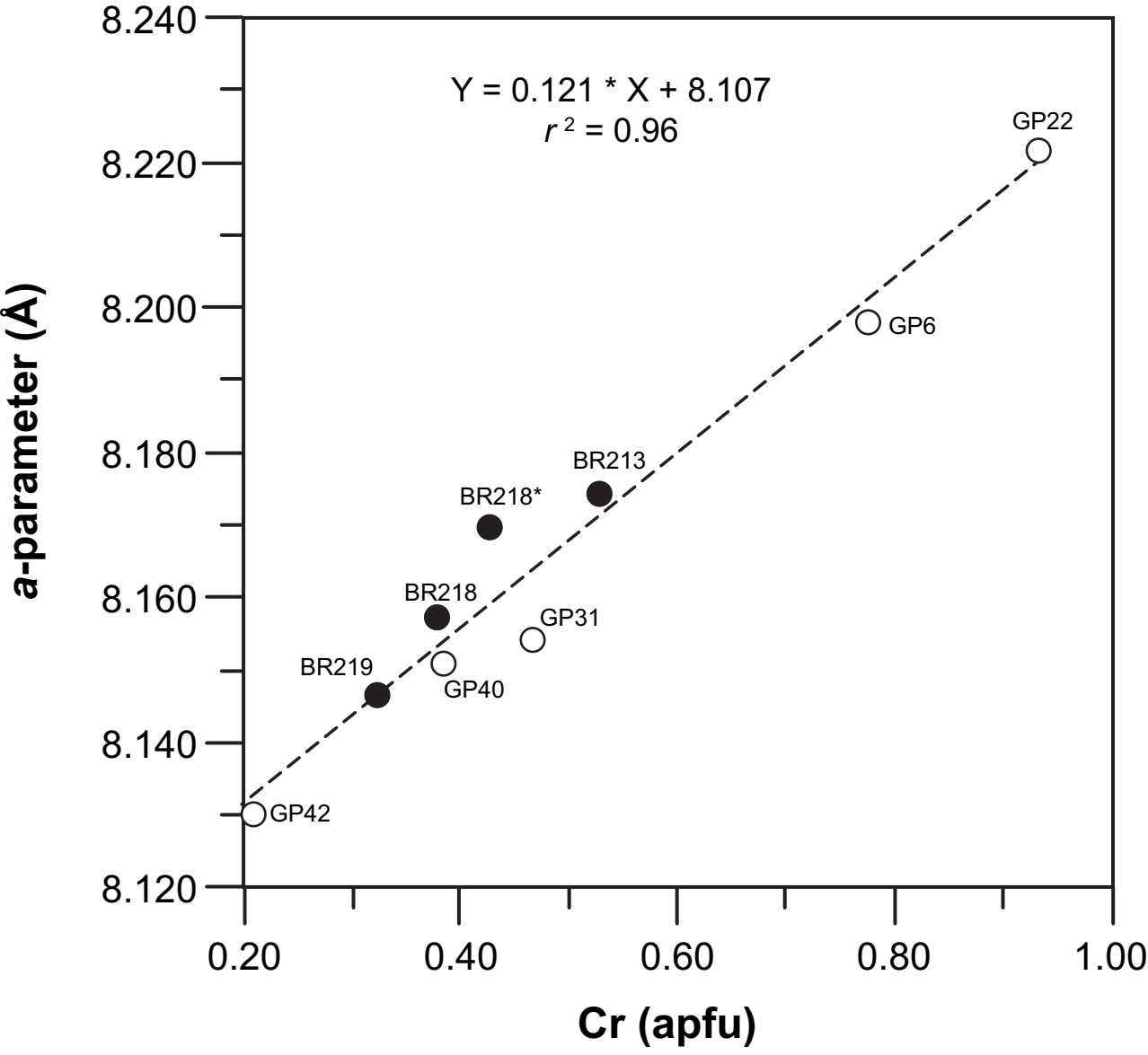
Y = 0.121 * X + 8.107
r 2 = 0.96
GP22
GP6
BR213
BR218*
BR218
GP31
BR219
GP40
GP42
8.240
8.220
8.200
8.180
8.160
8.140
8.120
0.20
0.40
0.60
0.80
1.00
a-parameter (Å)
Cr (apfu)

Figure 3

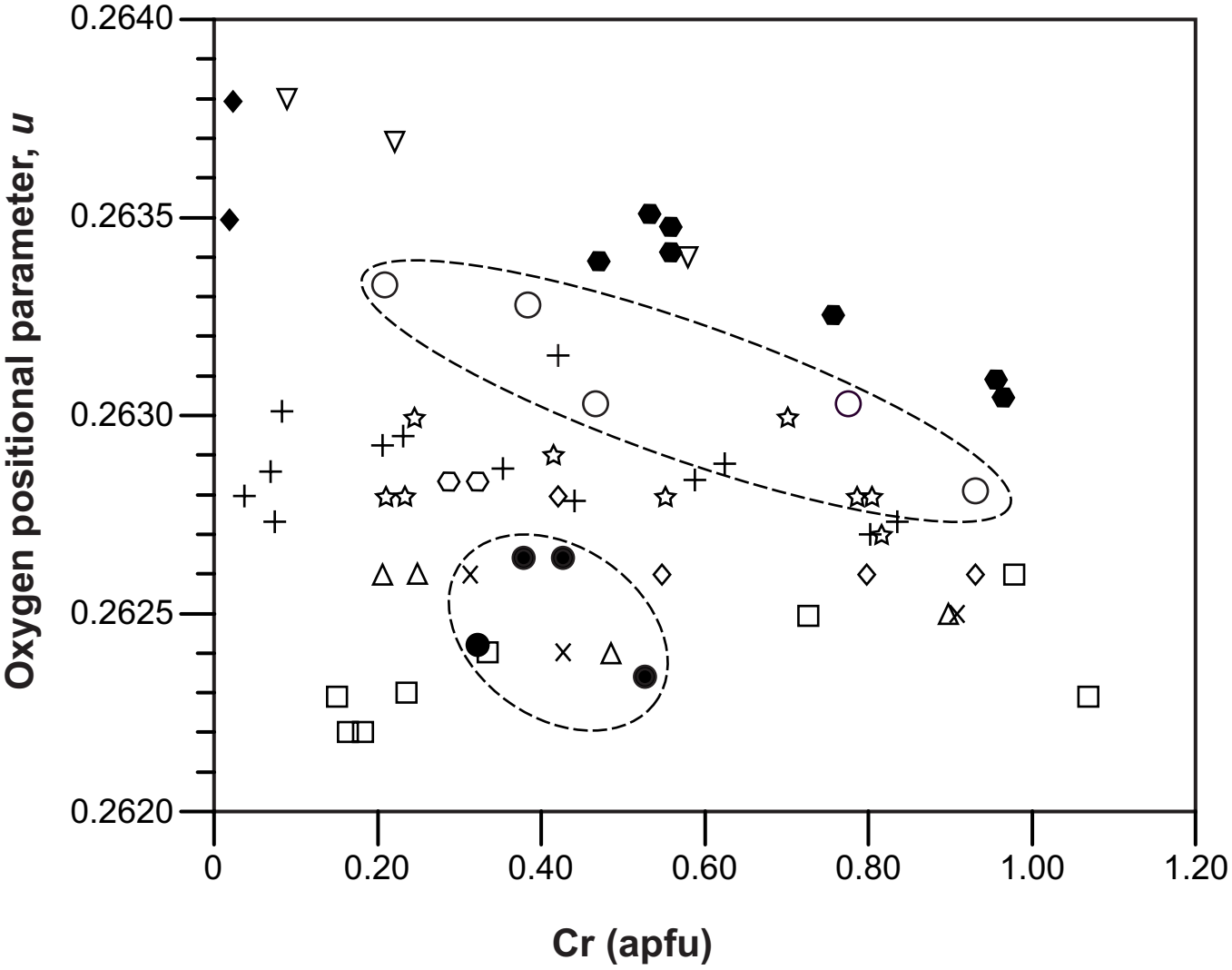

- ○ Greene Point
- ● Baker Rocks
- ⬢ Ronda massif (Lenaz et al. 2010)
- ▽ Balmuccia mantle peridotite and transitional dikes (Basso et al., 1984; Princivalle et al. 1989)
- ◆ Balmuccia Al-dikes (Basso et al., 1984; Menegazzo et al. 1997)
- □ Mt. Leura (Della Giusta et al. 1986)
- △ NE Brazil (Princivalle et al. 1989)
- ◇ Assab (Princivalle et al. 1989)
- × Mt. Noorat (Princivalle et al. 1989)
- ☆ Predazzo (Carraro 2003)
- + San Carlos (Uchida et al. 2005)
- ⬡ Hungary (Nédli et al. 2008)

Figure 4

TABLE 1 - Spinel-peridotite xenoliths from lithospheric mantle of northern Victoria Land selected for the present study

Sample	Rock type	Cr# in Spinel	*F*%	Type of metasomatism
GP6	harzburgite	0.39	15	cryptic
GP22	harzburgite	0.47	17	cryptic
GP31	harzburgite	0.24	10	cryptic
GP40	lherzolite	0.2	8	unmetasomatized
GP42	lherzolite	0.11	2	unmetasomatized
BR213	lherzolite	0.27	11	cryptic
BR218	lherzolite	0.19	8	cryptic
BR218*	lherzolite	0.22	9	Fe-Ti
BR219	harzburgite	0.16	6	cryptic

Notes: GP: Greene Point; BR: Baker Rocks; *: lherzolite portion adjacent to the amphibole-bearing vein crosscutting the xenolith; Cr#: Cr number expressed as Cr/(Cr+Al) atom; F%: degree of partial melting calculated using the Hellebrand et al. (2001) formulation based on the Cr# =[Cr/(Cr+Al)] ratio in spinel; Sp: spinel.

TABLE 2. Selected X-ray diffraction data of the spinels from northern Victoria Land

Crystal	GP6	GP22	GP31	GP40	GP42	BR213	BR218	BR218*	BR219
Crystal sizes (mm)	0.60×0.16×0.15	0.14×0.12×0.10	0.16×0.12×0.10	0.15×0.12×0.10	0.18×0.14×0.10	0.11×0.10×0.10	0.18×0.16×0.14	0.11×0.10×0.06	0.16×0.14×0.08
a (Å)	8.1983(2)	8.2219(1)	8.1544(3)	8.1509(1)	8.1304(2)	8.1743(2)	8.1573(3)	8.1695(1)	8.1466(2)
u	0.26303(5)	0.26281(3)	0.26303(3)	0.26328(4)	0.26333(3)	0.26234(4)	0.26264(4)	0.26264(4)	0.26242(4)
T-O (Å)	1.9600(7)	1.9625(5)	1.9495(5)	1.9523(5)	1.9480(4)	1.9445(5)	1.9447(6)	1.9475(5)	1.9391(5)
M-O (Å)	1.9486(3)	1.9558(2)	1.9382(2)	1.9355(3)	1.9303(2)	1.9480(3)	1.9417(3)	1.9446(3)	1.9407(3)
T-m.a.n.	15.39(7)	15.43(6)	14.57(5)	14.96(7)	14.56(5)	15.41(6)	16.17(10)	16.46(7)	15.19(5)
M-m.a.n.	17.55(6)	18.06(6)	15.55(5)	15.19(7)	14.27(3)	15.96(4)	15.26(10)	15.46(5)	14.99(4)
T-U^{11} (Å^2)	0.00645(14)	0.00648(10)	0.00644(11)	0.00613(13)	0.00585(10)	0.00644(10)	0.00665(12)	0.00687(10)	0.00614(10)
M-U^{11} (Å^2)	0.00472(8)	0.00447(6)	0.00488(7)	0.00468(10)	0.00452(7)	0.00479(7)	0.00492(10)	0.00493(7)	0.00488(7)
M-U^{12} (Å^2)	-0.00035(3)	-0.00033(3)	-0.00038(3)	-0.00032(3)	-0.00036(3)	-0.00027(3)	-0.00025(3)	-0.00029(3)	-0.00023(3)
O-U^{11} (Å^2)	0.00647(13)	0.00690(10)	0.00697(9)	0.00676(12)	0.00645(8)	0.00832(10)	0.00824(13)	0.00862(10)	0.00840(10)
O-U^{12} (Å^2)	-0.00077(9)	-0.00079(7)	-0.00046(6)	-0.00062(7)	-0.00045(6)	-0.00029(8)	-0.00027(8)	-0.00029(8)	-0.00013(8)
Reciprocal space range *hkl*	$-16 \le h \le 15$	$-13 \le h \le 13$	$-15 \le h \le 12$	$-15 \le h \le 12$	$-16 \le h \le 8$	$-16 \le h \le 15$	$-3 \le h \le 16$	$-14 \le h \le 14$	$-16 \le h \le 11$
	$-11 \le k \le 12$	$-14 \le k \le 16$	$-14 \le k \le 12$	$-15 \le k \le 10$	$-12 \le k \le 14$	$-13 \le k \le 10$	$-15 \le k \le 14$	$-14 \le k \le 14$	$-11 \le k \le 14$
	$-16 \le l \le 11$	$-16 \le l \le 12$	$-16 \le l \le 13$	$-15 \le l \le 16$	$-16 \le l \le 10$	$-8 \le l \le 16$	$-15 \le l \le 16$	$-16 \le l \le 16$	$-16 \le l \le 12$
EXTI	0.014(1)	0.0133(5)	0.038(1)	0.048(2)	0.021(1)	0.0062(5)	0.021(1)	0.0039(5)	0.0074(5)
Total reflections	2633	2668	2794	2749	2653	2709	2546	2781	2550
Unique reflections	133	139	135	136	135	137	136	138	135
R int. (%)	1.85	1.68	2.11	1.93	2.10	1.18	1.30	1.31	1.25
*R*1 (%) all reflections	1.17	0.75	0.83	0.99	0.82	0.95	1.06	0.96	0.99
*wR*2 (%) all reflections	3.09	1.94	2.04	2.52	2.21	2.38	2.61	2.38	2.23
GooF	1.217	1.338	1.207	1.300	1.308	1.216	1.190	1.222	1.205
Diff. Peaks (±*e*/Å^3)	–0.38; 0.36	–0.18; 0.17	-0.19; 0.15	-0.20; 0.15	-0.17; 0.17	-0.23; 0.20	-0.28; 0.24	-0.22; 0.26	-0.22; 0.20

Notes: *a* = unit-cell parameter; *u* = oxygen fractional coordinate; T-O and M-O = tetrahedral and octahedral bond lengths, respectively; T- and M-m.a.n.. = T- and M-mean atomic number; U^{11} = atomic displacement parameter; $U^{11} = U^{22} = U^{33}$ and $U^{12} = U^{13} = U^{23}$ (= 0 for *T*-site due to symmetry reasons); EXTI = extinction parameter; *R* int. = merging residual value; *R*1 = discrepancy index, calculated from *F*-data; *wR*2 = weighted discrepancy index, calculated from F^2-data; GooF = goodness of fit; Diff. Peaks = maximum and minimum residual electron density. Radiation, Mo-$K\alpha$ = 0.71073 Å. Data collection temperature = 293 K. Total number of frames = 1500. Range for data collection 8° < 2θ < 91°. Origin fixed at $\bar{3}m$. Space group $Fd\bar{3}m$. *Z* = 8 formula units. Spinel structure has cations at Wyckoff positions 8*a* ≡ T (1/8, 1/8, 1/8) and 16*d* ≡ M (1/2, 1/2, 1/2), and oxygen anions at 32*e* (*u*, *u*, *u*).

TABLE 3. Chemical composition (% in weight) of spinels from northern Victoria Land

Crystal	GP6	GP22	GP31	GP40	GP42	BR213	BR218	BR218*	BR219
SiO_2	0.06(3)	0.04(2)	0.05(1)	0.16(7)	0.06(3)	0.04(1)	0.03(1)	0.04(2)	0.03(1)
TiO_2	0.03(1)	0.08(4)	0.09(2)	0.10(4)	0.14(4)	0.10(3)	0.13(3)	0.50(2)	0.22(4)
Al_2O_3	36.26(13)	30.56(9)	47.68(2)	50.32(39)	58.07(4)	43.30(2.14)	50.14(18)	46.99(11)	52.27(8)
Cr_2O_3	35.15(37)	40.98(20)	21.92(11)	18.29(5)	10.45(1)	24.11(27)	17.85(12)	19.75(8)	15.38(13)
FeO	11.12(3)	11.86(17)	9.85(12)	11.04(30)	10.26(16)	12.35(19)	14.39(16)	15.54(2)	11.43(1)
MgO	17.69(17)	16.83(23)	19.02(13)	19.73(11)	20.45(15)	18.81(1.90)	17.37(2)	16.69(4)	19.67(33)
NiO	0.21(3)	0.18(6)	0.30(8)	0.32(5)	0.38(4)	0.21(3)	0.30(4)	0.26(4)	0.33(5)
$FeO^{\lozenge}$	7.23	8.90	6.80	9.16	8.00	10.50	12.37	13.52	9.83
$Fe_2O_3^{\lozenge}$	4.32	3.30	3.40	2.09	2.51	2.06	2.24	2.25	1.78
Total	100.95	100.86	99.26	100.17	100.06	99.14	100.43	99.99	99.49
Cations on the basis of 4 oxygen atoms per formula unit (apfu)									
Si^{4+}	0.002(1)	0.001(1)	0.002(1)	0.004(2)	0.002(1)	0.001(1)	0.001(1)	0.001(1)	0.001(1)
Ti^{4+}	0.001(1)	0.002(1)	0.002(1)	0.002(1)	0.003(1)	0.002(1)	0.003(1)	0.010(1)	0.004(1)
Al^{3+}	1.192(5)	1.035(5)	1.512(3)	1.573(7)	1.758(4)	1.411(52)	1.586(4)	1.515(2)	1.634(7)
Cr^{3+}	0.775(7)	0.931(5)	0.466(2)	0.384(2)	0.212(1)	0.527(19)	0.379(2)	0.427(2)	0.322(3)
Fe^{3+}	0.091(1)	0.071(1)	0.069(1)	0.042(1)	0.048(1)	0.043(2)	0.045(1)	0.046(1)	0.036(1)
Fe^{2+}	0.169(1)	0.214(3)	0.153(3)	0.203(5)	0.172(3)	0.243(9)	0.278(3)	0.309(1)	0.218(1)
Mg^{2+}	0.735(6)	0.721(8)	0.763(4)	0.780(5)	0.783(5)	0.775(6)	0.695(2)	0.680(2)	0.778(10)
Ni^{2+}	0.005(1)	0.004(1)	0.007(2)	0.007(1)	0.008(1)	0.005(1)	0.007(1)	0.006(1)	0.007(1)
Total cations	2.969	2.979	2.973	2.995	2.986	3.006	2.992	2.995	2.999
Vacancy	0.031	0.021	0.027	0.005	0.014	-	0.008	0.005	0.001
Σe^{-}_{EMPA}	49.83	52.03	46.02	45.68	43.38	47.91	46.68	47.75	45.20
Σe^{-}_{SREF}	50.48	51.55	45.67	45.35	43.11	47.33	46.69	47.39	45.18
Δe^{-}	0.65	0.48	0.34	0.33	0.27	0.57	0.01	0.36	0.02

Notes : Digits in brackets are estimated uncertainties (1σ): for reported oxide concentrations, they represent standard deviations of several analyses on individual crystals, while, for cations, they were calculated according to error propagation theory. Σe^{-}_{EMPA} and Σe^{-}_{SREF} = number of electrons per formula unit (epfu) derived from chemical and structural analysis, respectively; Δe = absolute deviation between e^{-}_{EMPA} and e^{-}_{SREF};
◊ = Determined on the basis of Mössbauer spectroscopy analysis, errors on Fe^{3+}/Fe_{tot} ratios estimated at maximum ± 0.03 (Perinelli et al., 2012).

TABLE 4. Cation site distribution (apfu), inversion and end-member compositions (%) for spinels from northern Victoria Land

	GP6	GP22	GP31	GP40	GP42	BR213	BR218	BR218*	BR219
T site									
Si	0.002	0.001	0.002	0.004	0.002	0.001	0.001	0.001	0.001
Al	0.036	0.029	0.088	0.078	0.103	0.126	0.136	0.125	0.161
Fe^{3+}	0.082	0.073	0.069	0.041	0.048	0.043	0.045	0.046	0.035
Fe^{2+}	0.169	0.190	0.136	0.175	0.143	0.197	0.233	0.261	0.181
Mg	0.680	0.687	0.679	0.697	0.692	0.633	0.576	0.563	0.622
Vacancy	0.031	0.022	0.027	0.005	0.014	0.000	0.008	0.005	0.001
Total T	1.000	1.000	1.000	1.000	1.001	1.000	1.000	1.000	1.001
M site									
Ti	0.001	0.002	0.002	0.002	0.003	0.002	0.003	0.010	0.004
Al	1.138	0.996	1.425	1.498	1.652	1.283	1.444	1.385	1.474
Cr	0.791	0.938	0.466	0.382	0.212	0.539	0.382	0.428	0.321
Fe^{3+}	0.009	0.000	0.000	0.000	0.000	0.000	0.000	0.000	0.000
Fe^{2+}	0.000	0.027	0.017	0.023	0.030	0.029	0.048	0.050	0.037
Mg	0.057	0.034	0.085	0.087	0.095	0.141	0.118	0.121	0.158
Ni	0.005	0.004	0.007	0.007	0.008	0.005	0.007	0.006	0.007
Total M	2.000	2.000	2.000	2.000	2.000	2.000	2.000	2.001	2.000
Inversion	0.06	0.07	0.11	0.12	0.13	0.18	0.17	0.18	0.20
End-member									
$MgAl_2O_4$	61	53	77	80	80	70	70	69	78
$FeCr_2O_4$	17	21	15	19	7	24	18	21	16
$MgCr_2O_4$	14	20	1	0	0	2	0	0	0
$FeAl_2O_4$	0	0	0	1	10	0	10	8	4
AB_2O_4	8	5	7	0	3	5	1	2	2

Notes: apfu = atoms per formula unit; inversion parameter calculated as the number of divalent cations at the M site.

TABLE 5 – Calculated intracrystalline closure temperature (T_c) *versus* intercrystalline equilibrium temperature (T) of spinel-peridotite xenoliths from lithospheric mantle of northern Victoria Land selected for this study

Sample	T_c (°C)	T (°C)
GP6	612	1032
GP22	639	1048
GP31	675	1109
GP40	592	985
GP42	594	1113
BR213	911	907
BR218	883	911
BR218*	891	927
BR219	899	933

Notes: T_c by the relation of Princivalle et al. (1999); T by the olivine-spinel geothermometer of Ballhaus et al. (1991), data from Perinelli et al. (2012). The uncertainty of ±20°C is associated to both methods.